THE JOURNAL OF PHYSICAL CHEMISTRY C

ARTICLE

pubs.acs.org/JPCC

Effective Heat Transfer Properties of Graphene Sheet Nanocomposites and Comparison to Carbon Nanotube Nanocomposites

Khoa Bui,[†,‡] Hai M. Duong[4,§] Alberto Striolo,[†,‡] and Dimitrios V. Papavassiliou[†,‡,*]

[†]School of Chemical, Biological, and Materials Engineering, University of Oklahoma, Norman, Oklahoma, United States

[‡]Carbon Nanotube Technology Center (CANTEC), University of Oklahoma, Norman, Oklahoma, United States

[§]Department of Mechanical Engineering, National University of Singapore, Singapore

ABSTRACT: By incorporating nanoinclusions (carbon nanotubes, graphene sheets) with exceptional thermal conductivity into a polymer matrix, one would expect to improve the heat performance of resulting nanocomposites. However, the effective thermal conductivity of carbon-based nanocomposites is strongly influenced by the Kapitza interfacial resistance. In this study, a comparison between carbon nanotubes and graphene sheet nanocomposites that takes into account dispersion patterns of the nanoinclusions and the Kapitza resistance is performed by means of a Monte Carlo simulation. It is found that graphene-based nanocomposites can be more efficient thermal conductors than carbon nanotube ones not only because of smaller Kapitza resistance but also because of the geometry of the graphene sheet. When the Kapitza resistance is reduced by appropriate functionalization of the graphene sheets and when the graphene sheet inclusions yield nematic patterns, our calculations suggest the possibility of obtaining composite materials with effective thermal conductivity up to 350 times larger in the direction parallel to the graphene sheets than in the direction perpendicular to them.

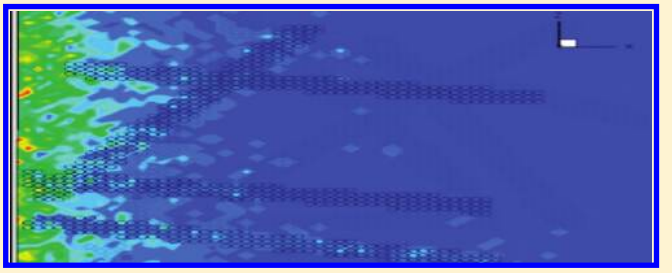

1. INTRODUCTION

Carbon nanotubes (CNTs) with their outstanding electrical, thermal, and mechanical properties have been suggested as reinforcement fillers in a variety of composite materials. By incorporating CNTs into a polymer matrix, or by dispersing CNTs into a solution, the effective thermal conductivity of the resulting composite can be increased. For example, this enhancement has been found to be from 80 to 125% at 1 wt % over pure polymer for the case of epoxy composites[1] or by a factor of almost 4 in the case of high volume fraction single-walled carbon nanotubes (SWNTs) in polystyrene.[2] However, on the basis of the properties of pure CNTs, one would expect a much higher increase of the effective thermal conductivity of such composite materials, up to an order of magnitude according to the classical theory of Maxwell. The presence of resistance to heat transfer at the CNT−polymer interface, known as the Kapitza interfacial thermal resistance, is the reason for this difference.

The value of the Kapitza resistance can be roughly estimated by the acoustic mismatch theory,[3] which attributed this resistance to phonon transport across the interface of dissimilar materials. The overall effective thermal conductivity of a system with nanoinclusions depends on the volume fraction of the nanoinclusions and on the interfacial thermal resistance. It has been suggested that the effective medium theory can provide insights about the thermal behavior of such systems[4,5] by taking into account the Kapitza resistance and different geometries of nanoinclusions. The effective thermal conductivity, K_{eff}, of CNT nanocomposites can also be calculated numerically with Monte Carlo (MC)-based methods, following the approach developed by Duong et al.[6] This method offers the advantage of explicitly accounting for the random or controlled placement of the CNTs, the Kapitza resistance between the CNTs and the matrix, and even the presence of a thermal boundary resistance between neighboring CNTs in contact with each other.[7,8] This method has been validated by comparisons to experimental data,[9] and it has also been used to estimate the Kapitza resistance effects for suspension systems.[10,11]

The nature of interfacial thermal resistance at the atomic scale can be explored with molecular dynamics (MD) simulations.[12−14] It has been reported that the overlap of the thermal vibration spectra between two materials is the key point to control the Kapitza resistance at the interface.[15,16] Multiscale modeling, in which the Kapitza resistance is examined by atomic-scale simulations and a meso/macroscopic approach is employed to study the thermal properties of bulk materials, can be seen as a suitable approach to this problem. Clancy et al.[13] employed MD simulations together with effective medium theory to study the effect of functionalization on Kapitza resistance and thermal conductivity

Received: October 18, 2010
Revised: January 17, 2011
Published: February 21, 2011

of resulting nanocomposites. They concluded that functionalization of edges and faces of nanoparticles is modestly effective in improving the thermal conductivity of the composite.

Graphene sheets (GS) have attracted attention because they are both cheaper[17] and possess properties analogous to those of CNTs.[18−20] Balandin et al.[21] reported extremely high values of the thermal conductivity of single-layer GS that outperform CNTs in terms of heat conduction. This result gives rise to the expectation that GS composites might be able to fulfill the promise of thermally conductive carbon-based nanocomposites. Recent theoretical and experimental investigations[22] suggest that electronic and magnetic properties of nano GS ribbons are strongly dependent on the edge structure. MD simulation studies investigated the thermal conductivity of graphene sheets with different edge terminations, and with different shapes. It was found that graphene nanoribbons have outstanding ballistic transport properties[23,24] and nanoribbons with zigzag long edges possess 125% higher thermal conductivity than that of armchair edges.[25,26] When CNT and GS are dispersed in organic mediums, the nanocomposite thermal conductivity will be affected by the Kapitza resistance. To minimize the Kapitza resistance, it has been suggested that functional groups, like alkane chains, should be covalently bonded to CNTs or GSs.[27−29]

While MD simulations have answered the question of whether GS has less Kapitza resistance than CNT or not,[15] the question of how much the macroscopic thermal properties of resulting nanocomposites are affected by the Kapitza resistance remains unanswered. In this work, we investigate the effective conductivity of GS nanocomposites by means of mesoscopic, off-lattice MC simulations. In addition to the presentation of a computational methodology for the study of the macroscopic effects of GS orientation, dispersion, and volume fraction on the effective thermal conductivity of GS nanocomposites, the contributions of this paper are: (a) a comparison of the macroscopic thermal performance between CNT nanocomposites, GS nanocomposites, and functionalized-GS nanocomposites and (b) the utilization of this methodology to calculate the Kapitza resistance of GS in polystyrene composites from recently conducted experiments. However, because of the coarse-grained level of description adopted herein, edge effects cannot be addressed.

2. SIMULATION METHODOLOGY AND SELECTION OF SIMULATION PARAMETERS

Details of the algorithm have been described in previous works.[6,9] Similar algorithms have been used for the simulation of heat or mass transfer in convective flows[30−33] and for the simulation of heat or mass transfer in porous media.[34,35] The heat transport is considered to be the result of the behavior of discrete heat walkers that travel through the composite by Brownian motion.[36] At each time step, the walkers move through the matrix with random jumps that are evaluated in each space direction by drawing random numbers from a normal distribution with a zero mean and a standard deviation, σ, given as

$$\sigma = \sqrt{2D_m\Delta t} \quad (1)$$

where D_m is the thermal diffusivity of the matrix material and Δt is the time increment of the simulation. Once a thermal walker arrives at the matrix−inclusion interface, it can either enter the inclusion based on a probability, designated as $f_{m\text{-}i}$, or remain in the matrix with a probability $(1 - f_{m\text{-}i})$. Once a walker moves inside an inclusion, it is assumed to distribute randomly and uniformly inside the inclusion, because the thermal conductivity of the inclusion (be it a CNT or a GS) is about 4 orders of magnitude larger than the thermal conductivity of the matrix. In every subsequent time step, the heat walker can exit the inclusion based on another probability, designated as $f_{i\text{-}m}$, that determines whether the walker will exit or will remain inside the inclusion, in which case it will be reassigned a new position inside the inclusion randomly. On the basis of thermal equilibrium, and assuming that the Kapitza resistance is the same when entering and when exiting the inclusion, the two probabilities, $f_{m\text{-}i}$ and $f_{i\text{-}m}$, are related as follows

$$V_i f_{i\text{-}m} = C_f \sigma A_i f_{m\text{-}i} \quad (2)$$

where A_i and V_i are the surface area and the volume of the inclusion, respectively, and C_f is a thermal equilibrium factor, which depends on the geometry of the inclusions.

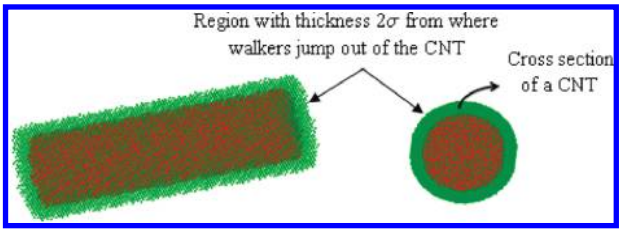

Figure 1. The thermal walkers can jump out of the inclusions by first arriving in a shell close to the inclusion−matrix interface (green area). This type of algorithm is computationally more efficient than letting walkers try to exit from anywhere inside the inclusion and at the same time ensures a continuous and uniform distribution of the walkers across the interface at thermal equilibrium.

In the present work, instead of placing the walkers at the CNT−matrix interface before moving them out of the CNT,[6] the exiting walkers are randomly placed inside a shell whose outer surface is the inclusion−matrix interface. The thickness of this shell is determined by the standard deviation of the Brownian motion movement, equal to 2σ. The walkers jump out of the inclusion after being placed randomly inside that shell (see Figure 1). For the GS, which is very thin, the walkers jump out from their locations inside the GS, again without first being moved to the inclusion surface. This scheme results to a uniform and continuous distribution of the walker density inside and outside the inclusions, even across the interface, at conditions of thermal equilibrium. In prior versions of the algorithm there was a discontinuity of the walker density across the interface at thermal equilibrium conditions, which was incorporated into the value of C_f. The new algorithm is, therefore, physically more sound.

The numerical methodology for calculating the thermal equilibrium factor, $C_f = 0.35$, for CNTs has been described by Duong et al.[6,9,11] The factor C_f is obtained as follows for a GS: First, one parallelepiped (representing a large GS) having dimensions of 2.52 nm × 64.45 nm × 0.34 nm was placed randomly inside a cubic computational box with sides equal to 100 nm (300 × 300 × 300 grid points). Second, the heat walkers were released at every grid cell and were allowed to perform their random walk. The fraction of heat walkers inside the GS was calculated after increments of 500 time steps, and the simulation was stopped once this value did not change any longer with simulation time (equilibrium state). The correct value of the equilibrium factor of the GS ($C_f = 0.33$) was considered to have been reached when the volume fraction of the parallelepiped was

dx.doi.org/10.1021/jp109978x |J. Phys. Chem. C 2011, 115, 3872–3880

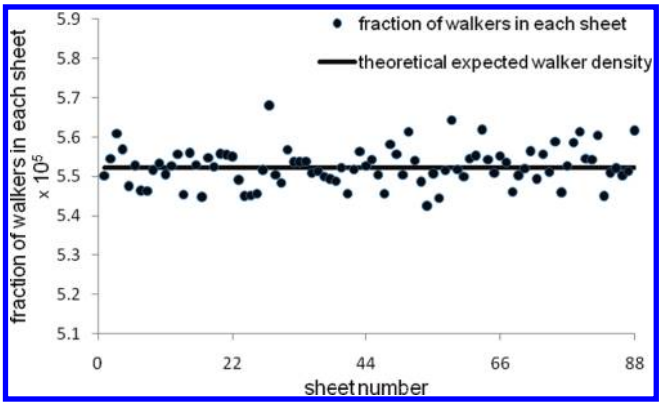

Figure 2. Fraction of walkers inside each GS with the sheet number (theoretically expected fraction of walkers) at thermal equilibrium state and $C_f = 0.33$. There are 88 sheets (2.52 nm × 64.45 nm × 0.34 nm) that are randomly dispersed inside a cubic computational domain with sides of 100 nm, so the fraction of the walkers within each sheet is expected to be equal to the volume fraction of one sheet ($2.52 \times 64.45 \times 0.34/1{,}000{,}000 = 5.52 \times 10^{-5}$). Because there is one heat walker released at every grid cell, the number of heat walkers in each GS at equilibrium will be equal to the number of grid cells constituting the GS, or in other words, the fraction of walkers staying inside the GS must be equal to the volume fraction of GS at thermal equilibrium conditions.

equal to the fraction of heat walkers inside the parallelepiped. Because there is one heat walker released at every grid cell at the beginning of the simulation, the number of heat walkers in each GS at equilibrium has to be equal to the number of grid cells constituting the GS, or in other words, the fraction of walkers staying inside the GS must be equal to the volume fraction of GS at thermal equilibrium conditions. Lastly, this value for C_f was checked further by placing 88 parallelepipeds (2.52 nm × 64.45 nm × 0.34 nm) randomly inside the same cubic computational box and examining the fraction of heat walkers inside each GS as compared to the expected value of this fraction. At thermal equilibrium, the heat walkers should distribute uniformly and the theoretically expected value of the fraction of the walkers inside all the GS should be equal to the volume fraction of the GS (Figure 2).

To estimate the effective thermal conductivity of a CNT or a GS nanocomposite, a cubic computational domain with sides of 100 nm and 300 × 300 × 300 equally spaced grid points was utilized. While the CNTs were simulated as solid cylinders, the GSs were considered as rectangular sheets, resembling GS nanoribbons. The thickness of the GS was equal to the distance between two graphite layers, which is 0.34 nm,[37] and the radius of the CNTs was 0.4 nm. Both the CNTs and the GSs were placed randomly inside the domain, with either random or controlled

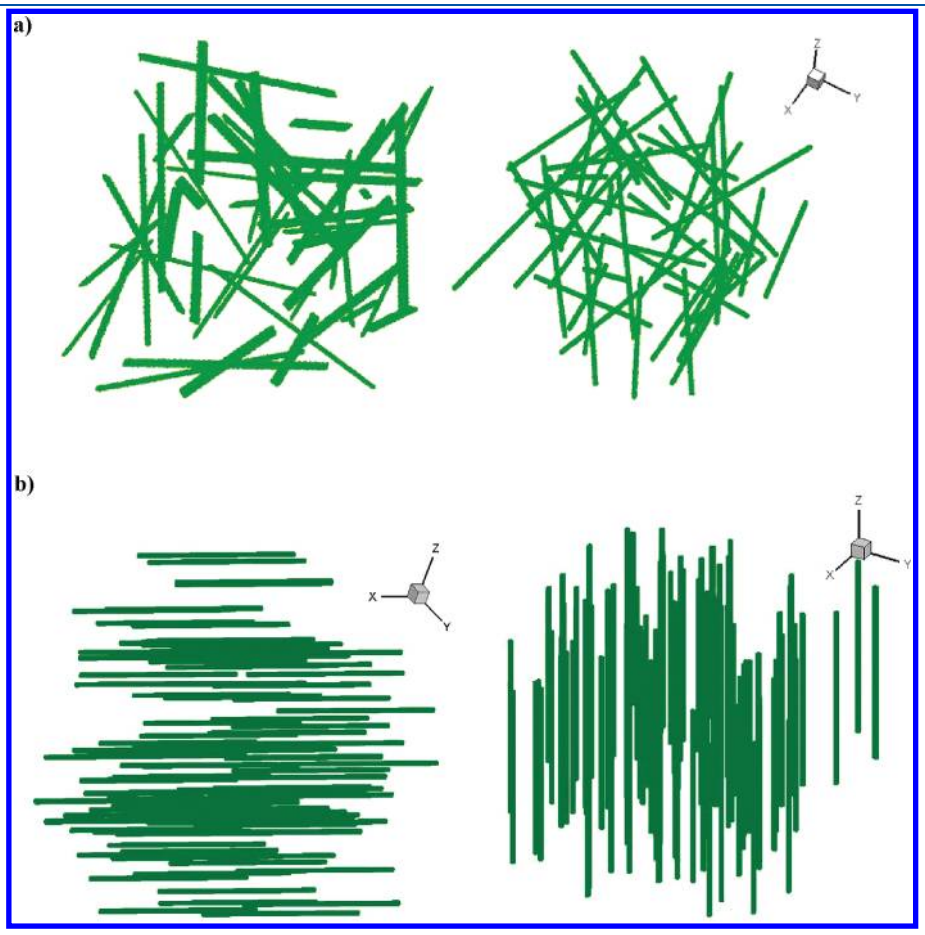

Figure 3. (a) 50 GSs (2.52 nm × 64.45 nm × 0.34 nm), left panel, and 50 CNTs (diameter = 0.8 nm, length = 64.45 nm, aspect ratio $L/d = 80.5$), right panel, that are randomly placed with random orientation inside a cubic computational domain with sides of 100 nm. (b) 100 CNTs (diameter = 0.8 nm, length = 64.45 nm, aspect ratio $L/d = 80.5$), right panel, that are placed parallel and perpendicular to the direction of heat flux (also x-direction) inside a cubic computational domain with sides of 100 nm.

dx.doi.org/10.1021/jp109978x |J. Phys. Chem. C 2011, 115, 3872–3880

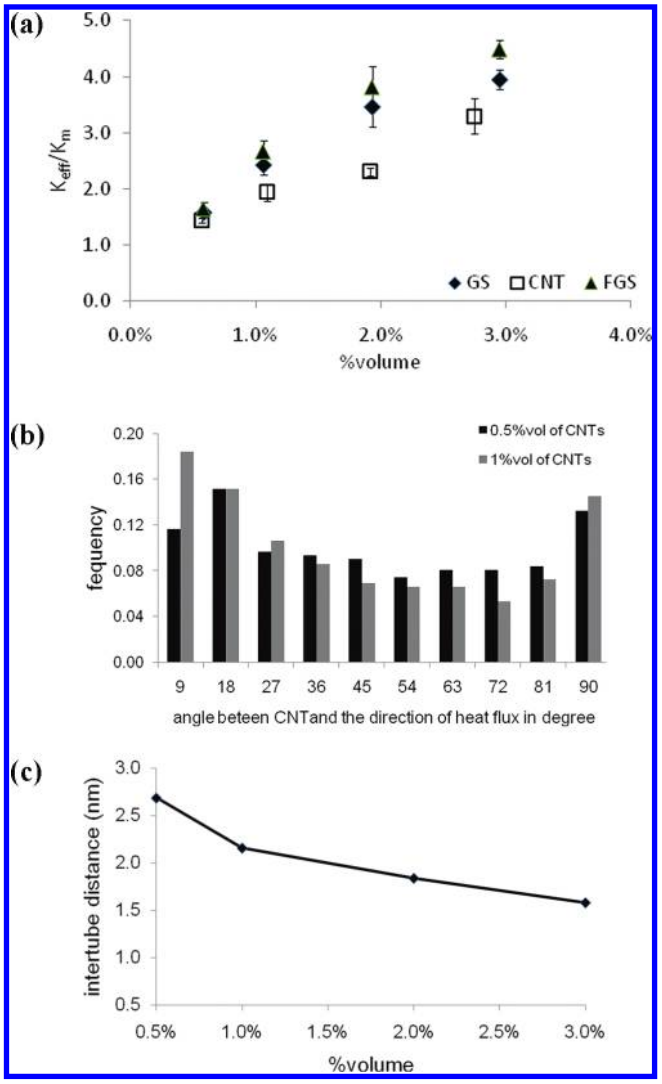

Figure 4. (a) Effective thermal conductivity of CNT composites (rectangles), GS composites (diamonds), and FGS composites (triangles) at various volume fractions. The inclusions are randomly placed with random orientation. The error bars indicate the variance of a *t* test with 95% level of confidence. (b) Distribution of the orientation of CNTs relative to the direction of the heat flux (i.e., *x* direction). The designation 0° means the CNTs are parallel to the *x* direction and 90° means the CNTs are perpendicular to *x* direction. (c) Change of average distance between six closest neighbor CNTs with the amount of CNTs inside the composite.

orientation relative to their axes, and were not in contact with each other (see Figure 3). Thermal walkers were released from one side of the computational domain, at $x = 0$, representing a heated surface. At the same time, an equal number (90,000) of cold walkers were released from the opposite plane, representing a cooled surface. The time step was equal to 10^{-4} s. The boundaries in the other two space directions were periodic. This scenario corresponds to the case of having a constant heat flux throughout the domain, and the temperature profile should be a straight line with a slope inversely proportional to the thermal conductivity of the composite. The temperature was obtained by counting the number of heat walkers in each grid unit after attaining steady state conditions and subtracting the number of heat walkers originating from the cold side of the box from the number of heat walkers originating from the hot side of the box.[38] Similar calculation protocols were implemented for the pure matrix, without any nanoparticles present, and for the nanocomposites with varying amounts of nanoparticles. The ratio between the temperature gradients without (i.e., when only the matrix was present in the domain) and with the inclusions is reported as the effective thermal conductivity of the nanocomposite divided by the thermal conductivity of the matrix (K_{eff}/K_m).

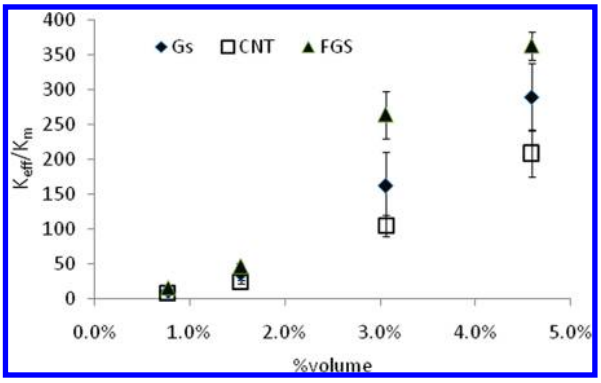

Figure 5. Effective thermal conductivity of CNT composites (rectangles), GS composites (diamonds), and FGS composites (triangles) at various volume fractions. The inclusions are randomly placed in the domain but are aligned in the *x* direction so that they are parallel to the heat flux.

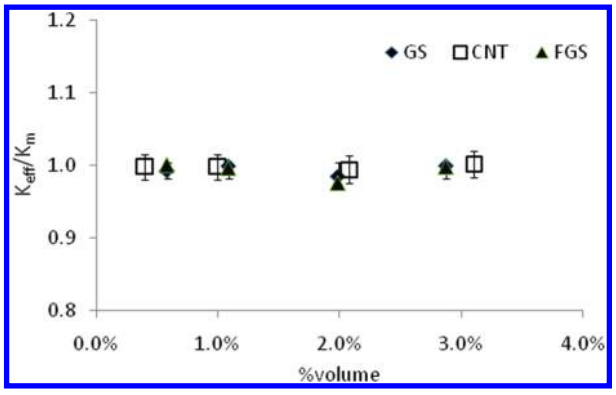

Figure 6. Effective thermal conductivity of CNT composites (rectangles), GS composites (diamonds), and FGS composites (triangles) at various volume fractions. The inclusions are randomly placed in the domain but are aligned in the *z* direction so that they are perpendicular to the heat flux. For the GS cases, the plane of each GS is normal to the direction of the heat flux.

The GSs were placed randomly within a cubic computational domain with the same size as the one described above. To create a randomly oriented GS, one needs to generate three different random angles corresponding to the rotation of the GS axis in the 3 directions of the Cartesian coordinate system. If the GS is required to be placed parallel or perpendicular to the *x*-axis (i.e., the axis parallel to the direction of heat flux), one can simply set the corresponding angle to be zero or $\pi/2$, respectively. For the case of CNTs, there are only two random angles required to generate randomly oriented cylinders. By changing the initial seed number used for the random number generator, the placement and orientation of the inclusions can be changed randomly. Following this procedure, six different simulation runs were conducted to obtain results for the conditions of

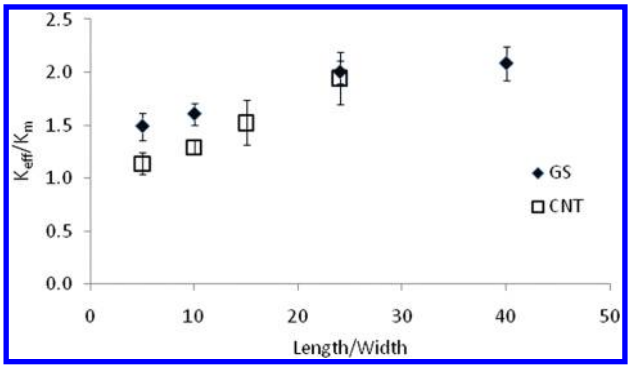

Figure 7. Effective thermal conductivity of CNT composites (rectangles) and GS composites (diamonds) at 1.0 % vol and different length/width ratios. The inclusions are randomly placed with random orientation.

each numerical experiment. The error bar that appears in Figures 4−7 represents the standard deviation of the results calculated using the Student's t test with a 95% level of confidence.

The value of the Kapitza resistance is a required input for the MC simulation. One can either estimate the Kapitza resistance based on a simplified theoretical approach (such as the acoustic mismatch model, AMM, or the diffuse mismatch model, DMM), or obtain it from experiment, or from MD simulations. It is also possible, if experimental values of the effective thermal conductivity of the nanocomposite are known, to use MC simulations in order to back calculate the Kapitza resistance for the nanocomposite. In the latter case, different values of the Kapitza resistance are assumed; the simulation is run for each case, and the correct Kapitza resistance is the one that yields results in agreement between the experiments and the simulations. Conventional numerical methods, like finite elements, have been used to obtain the conductivity for GS with a trial and error procedure when temperature data are available experimentally,[39] but the value of the Kapitza resistance cannot be obtained. When K_{eff} of a composite is studied, with our particle-based and meshless algorithm there is no need to generate a mesh that would fit the complicated geometry of inclusions dispersed into a matrix material and to repeat the mesh generation every time a new configuration is examined. Furthermore, the incorporation of the Kapitza resistance at the interfaces happens in a natural way, through a probability, which is according to the AMM theory one way to describe the Kapitza resistance.

According to the simplified AMM, the phonon transmission probability, $f_{m\text{-}i}$, is calculated from the Kapitza resistance as follows[3]

$$f_{m\text{-}i} = \frac{4}{\rho_m C_m \nu_m R_{bd}} \tag{3}$$

where subscript m designates the matrix and subscript i designates the inclusion, ρ is the density of the matrix material, C the specific heat, ν the velocity of sound in the matrix, and R_{bd} the Kapitza thermal boundary resistance. The probability $f_{m\text{-}i}$ can be found for the case when the incident wave is normal to the interface or as a function of incident angle according to[40]

$$f_{m\text{-}i}(\theta) = \frac{4\rho_m \nu_m \cos\theta_i \rho_i \nu_i \cos\theta_m}{(\rho_m \nu_m \cos\theta_i + \rho_i \nu_i \cos\theta_m)^2} \tag{4}$$

$$f_{m\text{-}i} = \int_0^{\pi/2} f_{m\text{-}i}(\theta) \cos\theta \sin\theta \, d\theta \tag{5}$$

where θ is the angle between the wave vector of the incident phonon and the vector normal to the interface, ν is the phonon velocity, and indices m and i refer to the matrix and the inclusion, respectively. The Kapitza resistance, based on the AMM model, is therefore calculated in two steps. First, based on Snell's Law[3]

$$\frac{\sin\theta_m}{\nu_m} = \frac{\sin\theta_i}{\nu_i} \tag{6}$$

one can replace

$$\cos\theta_i = \sqrt{1 - \left(\frac{\nu_i}{\nu_m}\sin\theta_m\right)^2} \tag{7}$$

and the phonon transmission probability as a function of incident angle θ_m in eq 4. Then, the average phonon transmission is calculated by eq 5 with numerical integration over the entire range of incident angles. Finally, the Kapitza resistance is obtained from eq 3.

The Kapitza resistance based on the DMM depends only on the phonon velocities inside the two materials and on the absolute temperature, T, as follows[3]

$$R_{bd} = \left(1.02 \times 10^{10} \frac{\nu_m^{-2}\nu_i^{-2}}{\nu_m^{-2} + \nu_i^{-2}}\right)^{-1} \times T^{-3} \tag{8}$$

Table 1 is a summary of the theoretical predictions for the values of the Kapitza resistance for a CNT−octane and a GS−octane suspension system. Suspensions in octane were chosen because MD simulation results are available[15,41] for CNTs, GSs, and functionalized GSs (FGS) in such systems. Because of computing power limitations, the MD simulations considered small GSs of 54−216 carbon atoms and FGS were obtained by attaching single or double alkane chains at the edges of these GSs.[15]

As can be seen in Table 1, not only do the AMM and the DMM approaches yield different values for the Kapitza resistance but their predictions also differ from those obtained from MD calculations. The AMM can provide an estimate but not a precise value of the Kapitza resistance, because it does not take into account phonon scattering events at the interface. The DMM assumes that all the phonons are diffusely scattered at the interface, or in other words, the incident phonon forgets where it came from and scatters in both media with the same energy. This diffuse scattering significantly decreases the Kapitza resistance at the interfaces, where the dissimilarity between two materials is extremely large. These theories cannot predict the Kapitza resistance for the case of functionalized GS, since the material properties appearing in eqs 3−8 are properties for pure substances. In light of these differences and the difficulty to obtain theoretical predictions for functionalized GS, Kapitza resistance values inspired by MD simulations were used as input for the CNT−matrix, GS−matrix, and FGS−matrix Kapitza resistances in the MC simulations. It should be pointed out here that MD results have also shown that the Kapitza resistance for GS systems depends on the GS size, so only comparisons to experiments will validate our assumptions. The average phonon transmission probability of SWNT−octane and GS−octane was

Table 1. Properties and Kapitza Resistance of SWNT and GS with and without Functional Groups in Octane[a]

composite	SWNT−octane	GS−octane	FGS−octane
$R_{bd} \times 10^8$ (m^2 K/W)			
AMM	1.32	5.33	
DMM	0.11	0.21	
MD[15,41]	4.26	1.33	0.42
	SWNT	GS	octane
K (W/mK)[21]	3000−3500	4840−5300	0.124
properties at 25 °C	heat capacity (J/kgK)	velocity of sound (m/s)	density (kg/m^3)
octane[27]	2230	1171	710
SWNTs[48,49]	670	17500	1400
GS[50]		20000	2230 (graphite)

[a] The Kapitza resistance was calculated based on the AMM and the DMM and with MD simulations.[15]

Table 2. Number of CNTs and GSs Used in the Simulation

	vol %						
	0.5	1.0	2.0	3.0	length (nm)	length/width	A_i/V_i
no. CNTs	155	310	620	930	64.45	25.6	5.03
no. GSs	88	176	352	528	64.45	25.6	6.70

calculated using eq 3. Furthermore, the results of Konatham and Striolo[41] indicate that FGS can be dispersed in octane, providing justification to our assumption that functionalized GSs do not agglomerate. By assumption of well-dispersed GS, GS−GS heat transfer resistances were not taken into account.

3. RESULTS AND DISCUSSION

3.1. GS Nanocomposites Compared to CNT Nanocomposites. For comparison purposes, the CNT and GS considered in our simulations have the same length. The width of one GS is equal to the perimeter of a CNT. The FGS is modeled as having the same geometric shape and dimensions as a GS, with the only difference being the value of the Kapitza resistance. Furthermore, in our calculations, a single value for the Kapitza resistance was assumed to apply everywhere at the interface between the matrix and the nanoinclusion, neglecting the effects of different GS edge types on the effective thermal conductivity. The number of CNTs and GSs used in each simulation run are presented in Table 2. Note that the volume of one CNT is smaller than that of one GS, so more CNTs are needed in order to keep the same volume percent as with GSs. In our simulations, the CNTs are considered as straight cylinders with diameter d = 0.8 nm and aspect ratio (length/width) = 80.5. By unfolding the CNTs, we obtained GSs with L/d = 25.6.

The values of the effective thermal conductivity are presented in Figure 4a as a function of the volume fraction of CNTs, GSs, and FGSs. The inclusions were randomly placed in the computational domain and also had random orientation (i.e., a random angle of the CNT axis relative to the Cartesian coordinate system and randomly oriented normal vectors to the GS planes). The inclusion placement algorithm worked sequentially, first randomly placing an inclusion and then checking whether this new inclusion intersected with previously placed inclusions. Also, for computational simplicity, neither GSs nor CNTs were allowed to intersect the faces of the computational box. Thus, despite the imposed random orientation, the distribution of the angles is not exactly uniform, but it is symmetric. As shown in Figure 4b for CNTs, the distribution of the orientation angles for the lower volume fraction case is closer to being uniform. As detailed later, the CNT orientation affects the effective nanocomposite thermal conductivity. The error bars in Figure 4a (and in other Figures) indicate the standard deviation in the results of 6 simulations conducted for each case using a Student t test with 95% level of confidence. As it can be seen, GS composites exhibit higher values of K_{eff} than CNT composites. This improvement is more obvious at larger volume fractions, where the use of functionalized GS can provide over 4 times enhancement of the thermal conductivity of the matrix. Our predictions show a significant enhancement of the thermal conductivity for GS-based nanocomposites. This result is due to several factors. In our calculations the Kapitza resistance is assumed to be smaller for GS and FGS than for CNT; the surface to volume ratio of one GS is 6.70, i.e., 33.3% higher than that of one CNT (Table 2).

The values of K_{eff} for the case of randomly placed inclusions, but with their longest dimension oriented in the direction of the heat flux, are presented in Figure 5 as a function of the volume fraction of CNTs, GSs, and FGSs. This is the case that yields the highest values of K_{eff}. With the same volume percent, the effective thermal conductivity of GS composites is roughly 50% higher than that of CNT composites, while FGS composites are predicted to have K_{eff} up to twice that of CNT composites.

Results in Figure 4a and in Figure 5 suggest that the effective thermal conductivity of all nanocomposites increases as the inclusion (CNT, GS, or FGS) volume fraction increases. It should be pointed out that for the calculations discussed herein the nanoinclusions are well dispersed within the organic matrix. As the inclusion volume fraction keeps increasing, the average distance between the nanoparticles decreases (see for example Figure 4c for CNT composites), and the nanoparticles will eventually come in contact with each other. At those conditions the nanoparticle−nanoparticle Kapitza resistance may become important, as suggested by Maruyama et al.[42] and Duong et al.[8]

The above results for CNTs are compared with results obtained from effective medium theory and the same volume fraction and size of the CNTs. Details of the analytical formulas are described in the literature.[4,5] When the inclusions (CNTs, GSs) are oriented parallel to the direction of the heat flux (i.e., in the x direction) the effective thermal conductivity can be computed by the rule of mixing to be equal to the volume

Table 3. Effective Thermal Conductivity of CNT, GS−Octane, and Comparison with Theoretical Results (eqs 9−11) at Different Volume Fractions[a]

vol %	0.5	1.0	2.0	3.0
	K_{eff}/K_m of CNT−octane			
parallel, theory	121.96	242.92	484.85	726.77
parallel, simulation	8.35	24.62	105.23	209.09
random, theory	1.19	1.38	1.69	2.04
random, simulation	1.44	1.94	2.30	3.29
perpendicular, theory	1.01	1.02	1.04	1.06
perpendicular, simulation	0.99	0.99	0.99	1.00
	K_{eff}/K_m of GS−octane			
parallel, theory	196.56	392.12	783.24	1174.35
parallel, simulation	11.46	36.94	162.60	289.32
perpendicular, theory	1.00	1.01	1.02	1.03
perpendicular, simulation	0.99	0.99	0.98	0.99

[a] The dimensions of CNTs are as described in Table 2. For the case of randomly oriented CNTs, the simulation generates truly random cylinders and the analytical formula considers aligned cylinders with an angle ϕ relative to the heat flux that satisfies $\cos^2\phi = {}^1/_3$.

fraction of each phase multiplied by its thermal conductivity, as follows

$$K_{eff} = (1 - w)K_m + wK_p \quad (9)$$

where K_m and K_p are the thermal conductivity of the matrix and of the inclusions, respectively, and w is the volume fraction of the inclusions. When they are oriented perpendicular to the direction of the heat flux (i.e., in the z direction, see Figure 3b,) then[4]

$$K_{eff} = \frac{K_p K_m}{K_p - w\left(K_p - K_m - \frac{R_{bd}K_m}{L}K_p\right)} \quad (10)$$

where L is the length of the inclusions. When the CNTs (cylindrical inclusions) are randomly oriented, the thermal conductivity is assumed to be the same as that of aligned CNTs oriented with an angle ϕ relative to the direction of the heat flux, such that $\cos^2\phi = {}^1/_3$. The effective thermal conductivity is then given as[5]

$$K_{eff} = K_m[3 + w(\beta_x + \beta_z)]/[3 - w\beta_x] \quad (11)$$

with

$$\beta_x = 2(K_{11}^c - K_m)/(K_m + K_{ii}^c) \text{ and } \beta_z = K_{33}^c/K_m - 1 \quad (12)$$

$$K_{11}^c = \frac{K_p}{1 + \frac{2R_{bd}K_p}{d}} \text{ and } K_{33}^c = \frac{K_p}{1 + \frac{2R_{bd}K_p}{L}} \quad (13)$$

where d and L are the diameter and length of the cylindrical inclusions, respectively.

As seen in Table 3, the analytical results overestimate the effective thermal conductivity for the cylinders that are parallel to the heat flux and underestimate these values for the case of randomly oriented cylinders compared to the simulation results. The reason of this major discrepancy for cylinders parallel to the direction of heat transfer is that there exists a Kapitza resistance at the interfaces at both ends of the cylinders when the cylinders are parallel to the heat flux, but the analytical formula does not take into account this effect.

3.2. Anisotropic Heat Transfer in Nanocomposites with Controlled Morphology of CNTs, GSs, and FGSs. When the inclusions were perpendicular to the heat flux, (Figure 6), our results predict no enhancement in the thermal conductivity in any of the cases examined. The values obtained for K_{eff} even decreased proportionally to the amount of inclusions placed in the system. The anisotropy ratio of the effective thermal conductivities of the composites with inclusions oriented parallel and perpendicular to the heat flux ($K_{eff\text{-}x}/K_{eff\text{-}z}$, where $K_{eff\text{-}x}$ and $K_{eff\text{-}z}$ are the effective thermal conductivities in the direction of the heat flux and in the direction perpendicular to the heat flux, respectively) has values that are almost equal to $K_{eff\text{-}x}$, since $K_{eff\text{-}z}$ is almost one for all cases. This anisotropy ratio represents the ratio of the largest to the smallest eigenvalue of the effective thermal conductivity tensor, often called the *condition number* of the tensor. As the inclusion volume fraction increases, the anisotropy ratio increases, reaching a value of over 350 for FGS and 4.5 vol %. It becomes evident that a material will behave as a thermally conducting material in one direction and as thermal shield in another, if the inclusions are properly oriented. Such properties would be possible to obtain with advanced CNT composites that have high volume fraction of oriented CNTs,[43,44] but there is need for some experimental effort to produce nanocomposites with controlled orientation of the GS.

3.3. Effects of Aspect Ratio of CNTs and GSs. Each GS was considered as a rectangular sheet, in which the heat can travel along two directions parallel to the GS plane. On the contrary, the CNT was a cylinder that acted as an one-dimensional heat conducting inclusion, especially at high aspect ratios. To study this effect on K_{eff} of the composite, we simulated cases where the Kapitza resistance of the GS−matrix was set to be equal to that of the CNT−matrix resistance (as shown in Table 1). The simulations were performed at the same volume fraction (1.0%), with random inclusion orientation, but with different length/width ratios.

As the length/width ratio (or length/perimeter ratio for the case of the CNTs) was equal to 25.6 for a GS and a CNT, no difference in K_{eff} of the composites was observed (see Figure 7). At high length/width ratio, the width of the GS is rather small compared to its length, and the heat conduction along the length is dominant like that of the CNT. However, K_{eff} of GS composites is larger than that of CNT composites, when the width of the GS is comparable to its length, because the heat can travel along both directions in this case. Regarding the question of what type of composite would be more efficient for heat transfer, a CNT composite or a GS composite when the Kapitza resistance is the same for both, the answer depends on the length/width ratio (see Figure 7). The value of K_{eff}/K_m increases as the length/width ratio increases from 5 to 25. Above this value, our predictions do not indicate enhancement of the effective thermal conductivity for GS composites relative to CNTs. The inclusion type (CNTs or GSs) is only important in small length/width ratios.

It is also seen in Figure 7 that K_{eff} of both the GS and the CNT composites increases with increasing length/width ratio. It has been observed with the use of MD[45] that the thermal conductivity of both SWNT and GS is proportional to the length indicating purely ballistic heat conduction. Shiomi et al.[45] found that as the length of CNTs and GSs increases, the distribution of effective phonon mean free paths becomes broader, so that phonons with relatively long mean free paths cause an increase of the thermal

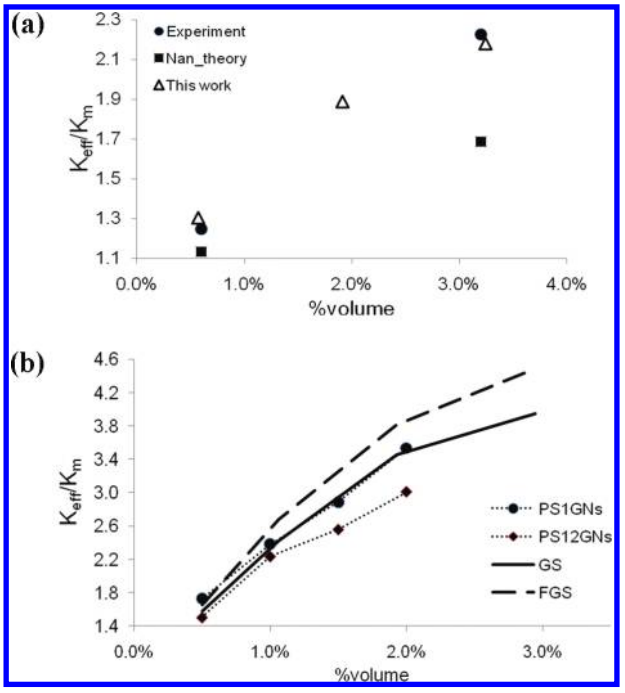

Figure 8. (a) Comparison of the enhancement factor (K_{eff}/K_m) of CNT−polyisoprene composite from experiment,[46] Nan's theory,[5] and this work. (b) Comparison of the enhancement factor (K_{eff}/K_m) of GS−octane (continuous line) and FGS−octane (dashed line) composites from this work with that of GS−PS composites from experiment[47] (the designations PS1GNs and PS12GNs correspond to low grafting density and high grafting density samples, respectively, following the symbols in Fang et al.).

conductivity. This also justifies our simulation approach to randomly and uniformly place the walkers once inside the inclusion, instead of moving them with Brownian movements, so long as the length of the nanoinclusions is larger than the phonon free path.

3.4. Comparison to Experimental Results. For CNT-based composites, validation of our protocol with comparison to experimental data has been described in our previous work.[9,10] Kapitza resistances were estimated for CNT−epoxy ($R_{bd} = 4.01 \times 10^{-8}$ m^2 K W^{-1}) and CNT−PMMA composites ($R_{bd} = 9.53 \times 10^{-9}$ m^2 K W^{-1}). On the basis of experimental data of CNT−polyisoprene composites[46] at 1 wt % (0.6 vol %), Kapitza resistance was calculated ($R_{bd} = 8.14 \times 10^{-8}$ m^2 K W^{-1}) by varying the value of $f_{m\text{-}i}$ in the MC simulations until K_{eff} from the simulations matched the experiment. By use of the Kapitza resistance thus obtained, we computed K_{eff} for CNT−polyisoprene composites at 5 wt % (3.2 vol %). As can be seen in Figure 8a, when the dispersion pattern of the CNTs is assumed to be the same at 1 and 5 wt % CNTs within the nanocomposite, our MC simulations reproduce the experimental data even better than the effective medium theory from Nan et al.[4,5]

A recent experimental report for GSs dispersed in polystyrene (GS−PS) at loadings less or equal to 2 wt % substantiates the conclusion that GS nanocomposites are better thermal conductors than SWNT nanocomposites.[47] This report did not include an estimation of the Kapitza resistance at the GS−PS interface. However, by comparing the enhancement factor, K_{eff}/K_m, with our current work, we can obtain an estimate of the Kapitza resistance for the GS−PS system (Figure 8b). For the same type of nanoinclusions and dispersion pattern, the ratio of the thermal conductivity of the composite divided by that of the polymer is affected by the Kapitza resistance rather than the type of the matrix material (polystyrene or octane). It is reasonable to conclude that composites with the same K_{eff}/K_m should have comparable Kapitza resistance, when the volume fraction of the inclusions and the dispersion pattern are the same.

There is some uncertainty regarding the length/width ratio, the thickness and the dispersion pattern of the GSs used in the experiments, since the GSs can bend and even twist. However, based on Figure 7, we can see that the value of K_{eff}/K_m does not change dramatically (28.5%) when varying the length/width ratio of the GSs. Assuming a pattern of randomly dispersed and randomly oriented GSs, we can see in Figure 8 that the experimental data from Fang et al.[47] for PS1GNs (i.e., graphene sheets with very small fraction of PS grafting) have a similar enhancement factor to that of GS-octane for randomly oriented GSs of similar weight percent in the present work. The value of Kapitza resistance of GS as well as FGS used in our work is 1.33×10^{-8} and 0.42×10^{-8} m^2 K W^{-1}, respectively. The Kapitza resistance of GS−PS is, thus, comparable to that of GS−octane.

4. CONCLUSIONS

On the basis of prior work, the GS nanocomposites appear to have lower values of Kapitza resistance when compared to the CNT composites. By use of MC methods, we have calculated the effective thermal properties of GS nanocomposites taking into account this resistance, and we have found that they can become an alternative to CNT composites from both a financial and a technical point of view. Composites with functionalized GSs exhibit almost double K_{eff} relative to CNT composites for inclusions oriented it the direction of the heat flux. Furthermore, by comparison with experiment data,[46,47] we found that the Kapitza resistance for a CNT−polyisoprene and for a GS−PS system are 8.14×10^{-8} and 1.33×10^{-8} m^2 K W^{-1}, respectively.

The anisotropy ratio of the effective thermal conductivity tensor increases for GS nanocomposites, indicating that there is added value in pursuing the manufacturing of GS composites with controlled orientation of GS. Controlling the orientation of the GS in the composite can lead to the manufacturing of composites that have quite different thermal behavior in different directions. For example, for an anisotropy ratio of 350 (like the FGS case) the material can be a thermal insulator in one direction and have a thermal conductivity 350 times larger than in a direction perpendicular to that.

Finally, it appears that the two-dimensional heat transfer is not important for GS with an aspect ratio larger than 25 and that the most important factor that affects the effective thermal conductivity is the value of the Kapitza thermal boundary resistance.

AUTHOR INFORMATION

Corresponding Author
*E-mail: dvpapava@ou.edu.

ACKNOWLEDGMENT

This work was supported by the DoE-funded Center for Applications of Single-Walled Carbon Nanotubes (Award Register No. ER64239 0012293). We also acknowledge support by DOD-EPSCOR: FA9550-10-1-0031. Computations were

carried out at the OU Supercomputing Center for Education & Research (OSCER) utilizing a Dell Pentium4 Xeon64 Linux Cluster (topdawg.oscer.ou.edu) and at the National Center for Supercomputing Applications at the University of Illinois (NCSA) under TeraGrid allocations TG-CTS-090017 and TG-CTS080042 utilizing the NCSA SGI Altix.

REFERENCES

(1) Bryning, M. B.; Milkie, D. E.; Kikkawa, J. M.; Yodh, A. G. *Appl. Phys. Lett.* **2005**, *87*, 161909.
(2) Peters, J. E.; Papavassiliou, D. V.; Grady, B. P. *Macromolecules* **2008**, *41* (20), 7274–7277.
(3) Swartz, E. T.; Pohl, R. O. *Rev. Mod. Phys.* **1989**, *61*, 605.
(4) Nan, C.-W.; Birringer, R.; Clarke, D. R.; Gleiter, H. *J. Appl. Phys.* **1997**, *81* (10), 6692–6699.
(5) Nan, C. W.; Liu, G.; Lin, Y.; Li, M. *Appl. Phys. Lett.* **2004**, *85* (16), 3549.
(6) Duong, H. M.; Papavassiliou, D. V.; Lee, L. L.; Mullen, K. J. *Appl. Phys. Lett.* **2005**, *87*, 013101.
(7) Duong, H. M.; Yamamoto, N.; Papavassilliou, D. V.; Maruyama, S.; Wardle, B. L. *Nanotechnology* **2009**, *20* (15), 155702.
(8) Duong, H. M.; Yamamoto, N.; Bui, K.; Papavassiliou, D. V.; Maruyama, S.; Wardle, B. L. *J. Phys. Chem. C* **2010**, *114* (19), 8851–8860.
(9) Duong, H. M.; Papavassiliou, D. V.; Mullen, K. J.; Maruyama, S. *Nanotechnology* **2008**, *19*, 065702.
(10) Duong, H. M.; Papavassiliou, D. V.; Mullen, K. J.; Wardle, B. L.; Maruyama, S. *J. Phys. Chem. C* **2008**, *112*, 19860.
(11) Duong, H. M.; Papavassiliou, D. V.; Mullen, K. J.; Wardle, B. L.; Maruyama, S. *Int. J. Heat Mass Transfer* **2009**, *52* (23−24), 5591–5597.
(12) Shenogina, N.; Godawat, R.; Keblinski, P.; Garde, S. *Phys. Rev. Lett.* **2009**, *102*, 15.
(13) Clancy, T. C.; Frankland, S. J. V.; Hinkley, J. A.; Gates, T. S. *Int. J. Therm. Sci.* **2010**, *49* (9), 1555–1560.
(14) Schroder, C.; Vikhrenko, V.; Schwarzer, D. *J. Phys. Chem. A* **2009**, *113* (51), 14039–14051.
(15) Konatham, D.; Striolo, A. *Appl. Phys. Lett.* **2009**, *95* (16), 163105.
(16) Budaev, B. V.; Bogy, D. B. *SIAM J. Appl. Math.* **2010**, *70* (5), 1691–1710.
(17) http://www.idtechex.com/research/reports/carbon_nanotubes_and_graphene_for_electronics_applications_technologies_players_and_opportunities_000229.asp
(18) Stankovich, S.; Dikin, D. A.; Dommett, G. H. B.; Kohlhaas, K. M.; Zimney, E. J.; Stach, E. A.; Piner, R. D.; Nguyen, S. T.; Ruoff, R. S. *Nature* **2006**, *442* (7100), 282–286.
(19) Kim, H.; Abdala, A. A.; Macosko, C. W. *Macromolecules* **2010**, *43* (16), 6515–6530.
(20) Cai, D. Y.; Song, M. *J. Mater. Chem.* **2010**, *20* (37), 7906–7915.
(21) Balandin, A. A.; Ghosh, S.; Bao, W.; Calizo, I.; Teweldebrhan, D.; Miao, F.; Lau, C. N. *Nano Lett.* **2008**, *8* (3), 902–907.
(22) Enoki, T.; Kobayashi, Y.; Fukui, K.-I. *Int. Rev. Phys. Chem.* **2007**, *26* (4), 609–645.
(23) Munoz, E.; Lu, J. X.; Yakobson, B. I. *Nano Lett.* **2010**, *10* (5), 1652–1656.
(24) Areshkin, D. A.; Gunlycke, D.; White, C. T. *Nano Lett.* **2006**, *7* (1), 204–210.
(25) Hu, J.; Ruan, X.; Jiang, Z.; Chen, Y. P. *AIP Conf. Proc.* **2009**, *1173* (1), 135–138.
(26) Hu, J.; Schiffli, S.; Vallabhaneni, A.; Ruan, X.; Chen, Y. P. *Appl. Phys. Lett.* **2010**, *97* (13), 133107.
(27) Huxtable, S. T.; Cahill, D. G.; Shenogin, S.; Xue, L.; Ozisik, R.; Barone, P.; Usrey, M.; Strano, M. S.; Siddons, G.; Shim, M.; Keblinski, P. *Nat. Mater.* **2003**, *2*, 731–734.
(28) Clancy, T. C.; Gates, T. S. *Polymer* **2006**, *47* (16), 5990–5996.
(29) Roy, A. K.; Farmer, B. L.; Sihn, S.; Varshney, V.; Patnaik, S.; Ganguli, S. *Diamond Relat. Mater.* **2010**, *19*, 268–272.
(30) Papavassiliou, D. V. *Int. J. Heat Mass Transfer* **2002**, *45*, 3571–3583.
(31) Mitrovic, B. M.; Le, P. M.; Papavassiliou, D. V. *Chem. Eng. Sci.* **2004**, *59* (3), 543–555.
(32) Le, P. M.; Papavassiliou, D. V. *J. AIChE* **2005**, *51* (9), 2402–2414.
(33) Verberg, R.; Alexeev, A.; Balazs, A. C. *J. Chem. Phys.* **2006**, *125* (22), 224712.
(34) Tomadakis, M. M.; Rupani, D. *J. Chem. Eng.* **2007**, *128* (1), 1–10.
(35) Voronov, R. S.; VanGordon, S. B.; Sikavitsas, V. I.; Papavassiliou, D. V. *Int. J. Num. Meth. Flu.* **2011**in press.
(36) Einstein, A. *Ann. Phys.* **1905**, *17*, 549.
(37) Huang, Y.; Wu, J.; Hwang, K. C. *Phys. Rev. B* **2006**, *74* (24), 245413.
(38) Papavassiliou, D. V.; Hanratty, T. J. *Int. J. Heat Mass Transfer* **1997**, *40* (6), 1303–1311.
(39) Ghosh, S.; Bao, W.; Nika, D. L.; Subrina, S.; Pokatilov, E.; Lau, C. N.; Balandin, A. A. *Nat. Mater.* **2010**, *9*, 555–558.
(40) Little, W. A. *Can. J. Phys* **1959**, *37* (3), 334–349.
(41) Konatham, D.; Striolo, A. *Nano Lett.* **2008**, *8* (12), 4630–4641.
(42) Maruyama, S.; Igarashi, Y.; Taniguchi, Y.; Shiomi, J. *J. Therm. Sci. Tech.* **2006**, *1* (2), 138–148.
(43) Garcia, E. J.; Wardle, B. L.; John Hart, A. *Composites A* **2008**, *39* (6), 1065–1070.
(44) Garcia, E. J.; Wardle, B. L.; John Hart, A.; Yamamoto, N. *Compos. Sci. Technol.* **2008**, *68* (9), 2034–2041.
(45) Shiomi, J.; Maruyama, S. *Int. J. Therm.* **2010**, *31* (10), 1945–1951.
(46) Tonpheng, B.; Yu, J.; Andersson, O. *Macromolecules* **2009**, *42* (23), 9295–9301.
(47) Fang, M.; Wang, K.; Lu, H.; Yang, Y.; Nutt, S. *J. Mater. Chem.* **2010**, *20* (10), 1982–1992.
(48) Yu, J.; Kalia, R. K.; Vashishta, P. *J. Chem. Phys.* **1995**, *103* (15), 6697–6705.
(49) Li, C.; Chou, T.-W. *Phys. Rev. B* **2006**, *73* (24), 245407.
(50) Hwang, E. H.; Das Sarma, S. *Phys. Rev. B* **2008**, *77* (11), 115449.